Monthly Notices
of the
ROYAL ASTRONOMICAL SOCIETY

Mon. Not. R. Astron. Soc. **425,** 1511–1520 (2012) doi:10.1111/j.1365-2966.2012.21675.x

The effect of ISM turbulence on the gravitational instability of galactic discs

Volker Hoffmann[1]★ and Alessandro B. Romeo[2]★

[1]*Institute for Theoretical Physics, University of Zürich, CH-8057 Zürich, Switzerland*
[2]*Onsala Space Observatory, Chalmers University of Technology, SE-43992 Onsala, Sweden*

Accepted 2012 July 5. Received 2012 July 5; in original form 2012 March 6

ABSTRACT

We investigate the gravitational instability of galactic discs, treating stars and cold interstellar gas as two distinct components, and taking into account the phenomenology of turbulence in the interstellar medium (ISM), i.e. the Larson-type scaling relations observed in the molecular and atomic gas. Besides deriving general properties of such systems, we analyse a large sample of galaxies from The H I Nearby Galaxy Survey (THINGS), and show in detail how interstellar turbulence affects disc instability in star-forming spirals. We find that turbulence has a significant effect on both the inner and the outer regions of the disc. In particular, it drives the inner gas disc to a regime of transition between two instability phases and makes the outer disc more prone to star-dominated instabilities.

Key words: instabilities – turbulence – ISM: kinematics and dynamics – ISM: structure – galaxies: ISM – galaxies: kinematics and dynamics.

1 INTRODUCTION

Today, 30 years after the pioneering work by Larson (1981), observations and simulations of the interstellar medium (ISM) are revealing its turbulent nature with higher and higher fidelity (see, e.g., Elmegreen & Scalo 2004; McKee & Ostriker 2007; Romeo, Burkert & Agertz 2010). A fundamental aspect of ISM turbulence is the existence of scaling relations between the mass column density (Σ), the 1D velocity dispersion (σ) and the size of the region over which such quantities are measured (ℓ):

$$\Sigma \propto \ell^a, \quad \sigma \propto \ell^b. \tag{1}$$

The values of a and b, and the range of scales spanned by ℓ depend on which ISM component we consider. In this paper, we focus on cold interstellar gas, which is highly supersonic and hence strongly compressible, and which is known to play an important role in the gravitational instability of galactic discs (e.g. Lin & Shu 1966; Jog & Solomon 1984a,b; Bertin & Romeo 1988, and references therein).

In the molecular gas, H_2, the scaling exponents are $a \approx 0$ and $b \approx \frac{1}{2}$, and equation (1) holds up to scales of a few 100 pc. In fact, both Galactic and extragalactic giant molecular clouds (GMCs) are fairly well described by Larson's scaling laws, $\Sigma =$ constant and $\sigma \propto \ell^{1/2}$, although the uncertainties are still large (e.g. Larson 1981; Solomon et al. 1987; Bolatto et al. 2008; Heyer et al. 2009; Hughes et al. 2010; Kauffmann et al. 2010; Lombardi, Alves & Lada 2010; Sánchez et al. 2010; Azimlu & Fich 2011; Ballesteros-Paredes et al. 2011; Field, Blackman & Keto 2011; Kritsuk & Norman 2011; Roman-Duval et al. 2011; Beaumont et al. 2012). Besides, Larson-type scaling relations have now been observed, for the first time, in the dense star-forming clumps of a high-redshift galaxy (Swinbank et al. 2011).

In the atomic gas, H I, the scaling exponents are instead $a \sim \frac{1}{3}$ and $b \sim \frac{1}{3}$, and equation (1) seems to hold up to scales of a few kpc. A Kolmogorov scaling for both σ and Σ is suggested by the observed power spectra of H I intensity fluctuations, and is also consistent with other measurements (e.g. Lazarian & Pogosyan 2000; Elmegreen, Kim & Staveley-Smith 2001; Begum, Chengalur & Bhardwaj 2006; Kim et al. 2007; Dutta et al. 2008; Roy, Peedikakkandy & Chengalur 2008; Dutta et al. 2009a,b; Block et al. 2010; Bournaud et al. 2010; Dutta et al. 2010; Dutta 2011; Combes et al. 2012; Zhang, Hunter & Elmegreen 2012). Note, however, that the uncertainties are larger than in the H_2 case. For example, high-resolution simulations of supersonic turbulence suggest a Burgers scaling for both σ and Σ, i.e. $a \sim \frac{1}{2}$ and $b \sim \frac{1}{2}$ (e.g. Fleck 1996; Kowal & Lazarian 2007; Kowal, Lazarian & Beresnyak 2007; Kritsuk et al. 2007; Schmidt, Federrath & Klessen 2008; Price & Federrath 2010). Other recent simulation surveys suggest that the scaling exponent a is significantly affected by turbulence forcing (Federrath, Klessen & Schmidt 2009; Federrath et al. 2010) and self-gravity (Collins et al. 2012).

In spite of such a burst of interest in ISM turbulence, and in spite of the dynamical importance of cold interstellar gas, there have been very few theoretical works aimed at evaluating the effect of turbulence on disc instability. In fact, traditional stability analyses do not take into account the scale dependence of σ (or Σ), but identify σ

★E-mail: volker@physik.uzh.ch (VH); romeo@chalmers.se (ABR)

with the typical 1D velocity dispersion observed at galactic scales. The first theoretical work devoted to the gravitational instability of turbulent gas discs was made by Elmegreen (1996), who assumed Larson-type scaling relations (see equation 1) and investigated the case $a = -1$ and $b = \frac{1}{2}$. He found that the disc is always stable at large scales and unstable at small scales. Romeo et al. (2010) also assumed Larson-type scaling relations, but explored the whole range of values for a and b. They showed that turbulence has an important effect on the gravitational instability of the disc: it excites a rich variety of stability regimes, several of which have no classical counterpart. See in particular the 'stability map of turbulence' (fig. 1 of Romeo et al. 2010), which illustrates such stability regimes and populates them with observations, simulations and models of interstellar turbulence.

In the gravitational instability of galactic discs, there is an important interplay between stars and cold interstellar gas (e.g. Agertz et al. 2009; Elmegreen 2011; Forbes, Krumholz & Burkert 2012; Cacciato, Dekel & Genel 2012). The gravitational coupling between these two components does not alter the form of the local stability criterion, $Q_{\rm eff} \geq 1$, but makes the effective Q parameter different from both the stellar and the gaseous Toomre (1964) parameters (Bertin & Romeo 1988; Romeo 1992, 1994; Elmegreen 1995; Jog 1996; Rafikov 2001; Shen & Lou 2003; Elmegreen 2011; Romeo & Wiegert 2011). The gravitational coupling between stars and gas also changes the least stable wavelength (Jog 1996), among other diagnostics.

What is the effect of ISM turbulence in this more realistic context? The first published attempt to answer this question was made by Shadmehri & Khajenabi (2012). They considered two-component discs of stars and turbulent gas, chose a and b so as to sample five of the seven stability regimes found by Romeo et al. (2010), and studied the dispersion relation numerically. Their study suggests that turbulence has a significant effect on disc instability even when stars are taken into account. The goal of our paper is to answer the question above in detail, extending previous work along two directions.

(i) We perform a rigorous stability analysis of two-component turbulent discs, motivated by observations of ISM turbulence in nearby galaxies. In particular, we consider two complementary cases: H I plus H_2, and gas plus stars. In the first case, we examine the dispersion relation analytically, and illustrate how the gravitational coupling between H I and H_2 modifies the main stability regimes of gas turbulence, which were originally derived neglecting such a coupling (Romeo et al. 2010). In the second case, we show that there are four stability regimes of galactic interest, similar to those analysed above, but in only one of them do stars play a non-negligible role. We then focus on such a regime and illustrate how gas turbulence affects the onset of gravitational instability in the disc, i.e. the local stability threshold and the corresponding characteristic wavelength.

(ii) We apply this analysis to a large sample of star-forming spirals from The H I Nearby Galaxy Survey (THINGS), previously analysed by Leroy et al. (2008) and Romeo & Wiegert (2011), and illustrate how ISM turbulence affects a full set of stability diagnostics: the condition for star–gas decoupling, the effective Q parameter and the least stable wavelength.

The rest of the paper is organized as follows. The (in)stability of two-component turbulent discs is analysed in Section 2, our application to THINGS spirals is shown in Section 3, the relation between our results and those of Shadmehri & Khajenabi (2012) is discussed in Section 4 and the conclusions are drawn in Section 5.

2 (IN)STABILITY OF TWO-COMPONENT TURBULENT DISCS

2.1 Summary of the one-component case

Here we summarize some of the results found by Romeo et al. (2010), which are fundamental to a proper understanding of Sections 2.2– 2.4.

The dispersion relation of a turbulent and realistically thick gas disc is

$$\omega^2 = \kappa^2 - 2\pi G \Sigma(k)\, k + \sigma^2(k)\, k^2, \tag{2}$$

where ω and k are the frequency and the wavenumber of the perturbation, and κ is the epicyclic frequency. $\Sigma(k)$ and $\sigma(k)$ are the mass column density and the 1D velocity dispersion measured over a region of size $\ell = 1/k$, as inferred from observations (see, e.g., Elmegreen & Scalo 2004; McKee & Ostriker 2007; Romeo et al. 2010):

$$\Sigma(k) = \Sigma_0 \left(\frac{k}{k_0}\right)^{-a}, \quad \sigma(k) = \sigma_0 \left(\frac{k}{k_0}\right)^{-b}. \tag{3}$$

If the disc has volume density ρ and scale height h, then $\Sigma \approx 2\rho\ell$ for $\ell \lesssim h$ and $\Sigma \approx 2\rho h$ for $\ell \gtrsim h$. The range $\ell \lesssim h$ corresponds to the case of 3D turbulence (GMCs and H I at small scales), whereas the range $\ell \gtrsim h$ corresponds to the case of 2D turbulence (H I at large scales). The quantity $\ell_0 = 1/k_0$ introduced in equation (3) is the fiducial scale at which Σ and σ are observed. This is also the scale at which the Toomre parameter Q and other stability quantities are measured, so that $Q_0 = \kappa\sigma_0/\pi G\Sigma_0$.

The scaling exponents a and b have an important effect on the shape of the dispersion relation (equation 2), and hence on the condition for local gravitational instability ($\omega^2 < 0$). As a and b vary, turbulence drives the disc across seven stability regimes, three of which are densely populated by observations, simulations and models of galactic turbulence (see fig. 1 of Romeo et al. 2010).

(i) For $b < \frac{1}{2}(1 + a)$ and $-2 < a < 1$ (hereafter *Regime A*), the stability of the disc is controlled by Q_0: the disc is stable at all scales if and only if $Q_0 \geq \overline{Q}_0$, where $\overline{Q}_0$ depends on a, b and ℓ_0. This is the domain of H I turbulence. Both H I observations and high-resolution simulations of supersonic turbulence are consistent with the scaling $a = b$. In such a case, the local stability criterion degenerates into $Q_0 \geq 1$, as if the disc were non-turbulent and infinitesimally thin.

(ii) For $b > \frac{1}{2}(1 + a)$ and $-2 < a < 1$ (hereafter *Regime C*), the stability of the disc is no longer controlled by Q_0: the disc is always unstable at small scales (i.e. as $k \to \infty$) and stable at large scales (i.e. as $k \to 0$).

(iii) For $b = \frac{1}{2}(1 + a)$ and $-2 < a < 1$ (hereafter *Regime B*), the disc is in a phase of transition between stability in the manner of Toomre (Regime A) and instability at small scales (Regime C). This is the domain of H_2 turbulence. Note, however, that even small deviations from Larson's scaling laws can drive the disc into Regime A or Regime C, and thus have a strong impact on its gravitational instability.

Since Regimes A–C are fundamental to a proper understanding of Sections 2.2– 2.4, we show them in Fig. 1. Note, however, that this simple figure is not meant to be a substitute for fig. 1 of Romeo et al. (2010), which illustrates all seven stability regimes and their relation to the phenomenology of ISM turbulence.

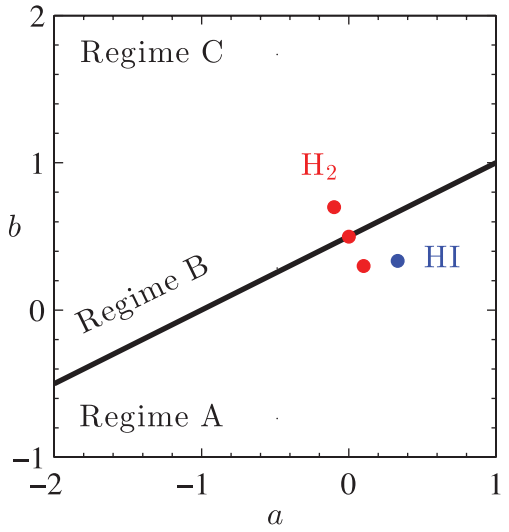

Figure 1. The main stability regimes of one-component turbulent discs (see Section 2.1). Also shown are the two-component cases illustrated in Fig. 2: H I in Regime A ($a_1 = b_1 = \frac{1}{3}$) plus H_2 in Regime A ($a_2 = 0.1$, $b_2 = 0.3$), Regime B ($a_2 = 0.0$, $b_2 = 0.5$) or Regime C ($a_2 = -0.1$, $b_2 = 0.7$).

2.2 Dispersion relation and general properties

Until now we have considered H I and H_2 separately. How does the stability scenario change when H I and H_2 are considered together? And how does it change when both gas and stars are taken into account? We will answer these questions here and in Sections 2.3 and 2.4.

When H I and H_2 are considered together, their gravitational coupling changes how the disc responds to perturbations. The dispersion relation can be expressed in a form that is particularly useful for discussing the stability properties of the disc:

$$\left(\omega^2 - \mathcal{M}_1^2\right)\left(\omega^2 - \mathcal{M}_2^2\right) = \left(\mathcal{P}_1^2 - \mathcal{M}_1^2\right)\left(\mathcal{P}_2^2 - \mathcal{M}_2^2\right), \tag{4}$$

where

$$\mathcal{M}_i^2 \equiv \kappa^2 - 2\pi G \Sigma_i(k)\, k + \sigma_i^2(k)\, k^2, \tag{5}$$

$$\mathcal{P}_i^2 \equiv \kappa^2 + \sigma_i^2(k)\, k^2, \tag{6}$$

and $i = 1, 2$.[1] Note that $\omega^2 = \mathcal{M}_i^2(k)$ is the one-component dispersion relation for potential-density waves (cf. equation 2), while $\mathcal{P}_i^2(k)$ describes sound waves modified by rotation (and turbulence). Since $\mathcal{M}_i^2(k)$–$\mathcal{P}_i^2(k)$ represents the self-gravity of component i, the right-hand side of equation (4) measures the strength of gravitational coupling between the two components.

Equations (4)–(6) are also applicable to two-component discs of gas and stars, even though the stellar component is collisionless and non-turbulent. This is because stars can be accurately treated as a fluid when analysing the stability of galactic discs (Bertin & Romeo 1988; Rafikov 2001), and because the equations above are valid whether each fluid is turbulent or not. Remember, in fact, that the phenomenology of turbulence is encapsulated in $\Sigma_i(k)$ and $\sigma_i(k)$ without altering the form of those equations. When the disc is made of gas (g) and stars ($\star$), $\Sigma_g(k)$ and $\sigma_g(k)$ are given by equation (3), while the stellar quantities are not. $\Sigma_\star(k)$ is the reduced surface density, $\Sigma_\star(k) = \Sigma_\star/(1 + kh_\star)$, where the k-dependent factor results from the finite scale height of the stellar layer (Vandervoort 1970; Romeo 1992, 1994; Elmegreen 2011). In contrast, $\sigma_\star$ is the radial velocity dispersion and does not depend on k, since the pressure term in the dispersion relation is unaffected by disc thickness (see again Vandervoort 1970). The gaseous and stellar Toomre parameters are then defined as $Q_{g0} = \kappa\sigma_{g0}/\pi G\Sigma_{g0}$ and $Q_\star = \kappa\sigma_\star/\pi G\Sigma_\star$.

As equation (4) is quadratic in ω^2, it can be solved with elementary methods. The discriminant is positive, so there are two real roots:

$$\omega_\pm^2 = \frac{1}{2}\left[\left(\mathcal{M}_1^2 + \mathcal{M}_2^2\right) \pm \sqrt{\Delta}\right], \tag{7}$$

$$\Delta = \left(\mathcal{M}_1^2 - \mathcal{M}_2^2\right)^2 + 4\left(\mathcal{P}_1^2 - \mathcal{M}_1^2\right)\left(\mathcal{P}_2^2 - \mathcal{M}_2^2\right). \tag{8}$$

This means that the dispersion relation has two branches that do not cross, $\omega_+^2(k) \neq \omega_-^2(k)$, except possibly as $k \to 0$ or $k \to \infty$. The functions $\omega_\pm^2(k)$ satisfy two basic properties, which constrain the gravitational instability of the disc and generalize the stability constraints found in the classical two-component case (Jog & Solomon 1984a; Bertin & Romeo 1988). Such properties are stated and proved below, and can easily be visualized with the help of Fig. 2. The cases illustrated represent a disc made of marginally stable H I (in Regime A) and unstable H_2 (in Regimes A–C).

(i) *Property I:* $\omega_-^2(k)$ lies below both $\mathcal{M}_1^2(k)$ and $\mathcal{M}_2^2(k)$, i.e. a two-component self-gravitating disc is more unstable (or less stable) than each component, whether this is turbulent or not. This can be proved by noting that Δ is larger than $(\mathcal{M}_1^2 - \mathcal{M}_2^2)^2$, so that $\sqrt{\Delta} > |\mathcal{M}_1^2 - \mathcal{M}_2^2|$. In turn, this implies that $\omega_-^2 < \mathcal{M}_{\rm min}^2$, where $\mathcal{M}_{\rm min}^2$ is the smallest $\mathcal{M}_i^2$ for a given k.

(ii) *Property II:* $\omega_+^2(k)$ is bounded by $\mathcal{P}_1^2(k)$ and $\mathcal{P}_2^2(k)$, i.e. this branch is always stable and represents sound waves modified by rotation (and turbulence). To prove this, note that the inequality $\sqrt{\Delta} > |\mathcal{M}_1^2 - \mathcal{M}_2^2|$ also implies that $\omega_+^2 > \mathcal{M}_{\rm max}^2$, where $\mathcal{M}_{\rm max}^2$ is the largest $\mathcal{M}_i^2$ for a given k. Note also that ω_+^2 cannot be smaller than $\mathcal{P}_{\rm min}^2$ or larger than $\mathcal{P}_{\rm max}^2$, otherwise equation (4) would not hold. Therefore, it must be $\mathcal{P}_{\rm min}^2 \leq \omega_+^2 \leq \mathcal{P}_{\rm max}^2$.

2.3 H I plus H_2

In Section 2.1, we have summarized the main stability regimes of one-component turbulent discs. Let us now extend the discussion to two-component discs of H I and H_2, analysing three cases of galactic interest (see again Fig. 2).

2.3.1 H_2 in Regime A

The response of each component is driven by pressure at small scales and by rotation at large scales, while self-gravity acts more strongly at intermediate scales (see section 2.7 of Romeo et al. 2010). This means that the gravitational coupling between the two components is negligible as $k \to 0$ and $k \to \infty$, and so is the right-hand side of equation (4). Therefore, the two branches of the dispersion relation behave asymptotically as $\mathcal{M}_1^2(k)$ and $\mathcal{M}_2^2(k)$, i.e. they converge to κ^2 as $k \to 0$ and diverge positively as $k \to \infty$. Since the potentially unstable branch $\omega_-^2(k)$ lies below $\mathcal{M}_i^2(k)$ (cf. Property I) and $\mathcal{M}_i^2(k)$ has a minimum for $k > 0$, $\omega_-^2(k)$ must also have a global minimum below κ^2. Thus, the disc is stable in the manner of Toomre, like each component (see the left-hand panel of Fig. 2).

[1] The dispersion relation of an N-component turbulent disc is $\sum_{i=1}^{N}(\mathcal{M}_i^2 - \mathcal{P}_i^2)/(\omega^2 - \mathcal{P}_i^2) = 1$, as can easily be inferred from equation 22 of Rafikov (2001). This equation cannot be expressed in a form similar to equation (4), and will not be used in the rest of the paper.

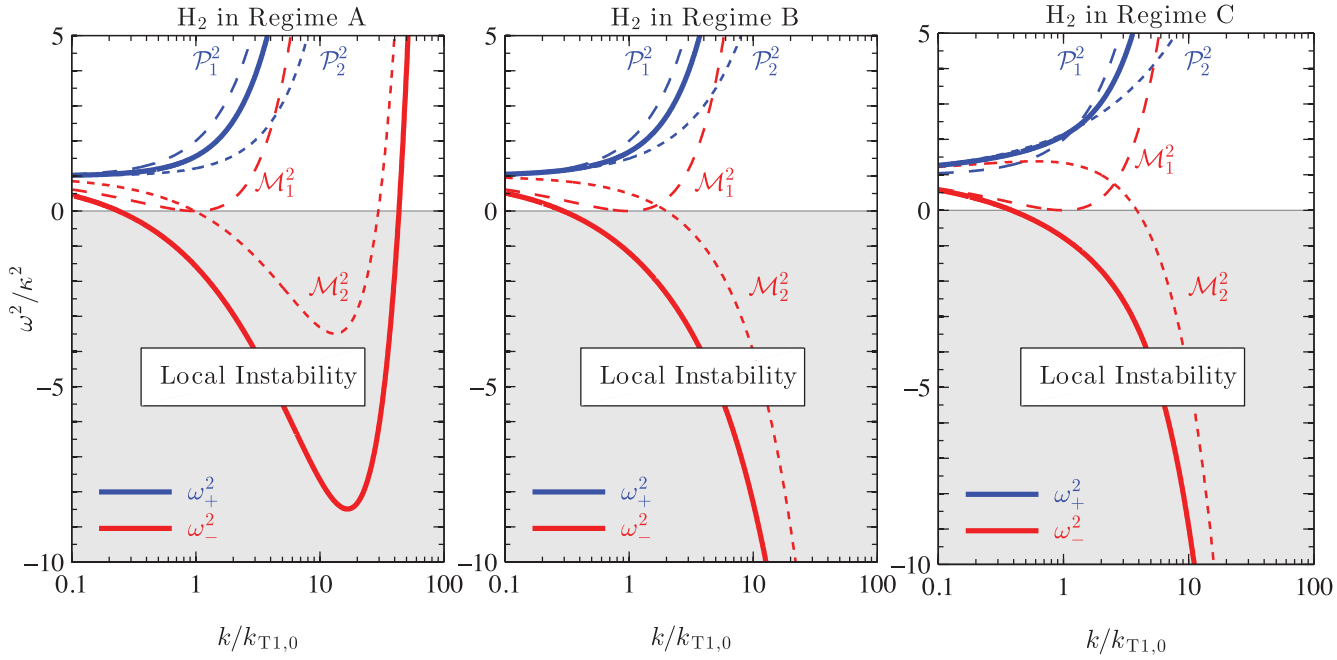

Figure 2. The two branches of the dispersion relation, $\omega_+^2(k)$ and $\omega_-^2(k)$, versus their one-component counterparts, $\mathcal{P}_i^2(k)$ and $\mathcal{M}_i^2(k)$, in stability regimes of galactic interest. These quantities are measured in units of κ^2, the square of the epicyclic frequency, while k is measured in units of $k_{T1,0} = \kappa^2/2\pi G\Sigma_{1,0}$, the Toomre wavenumber of component $i = 1$ at scale $\ell = \ell_0$. The cases illustrated represent a disc made of marginally stable H I (in Regime A) and unstable H_2 (in Regimes A–C). The scaling exponents are specified in Fig. 1. The other independent quantities are as follows: $k_0 = 8\,k_{T1,0}$, $Q_{1,0} = 1$, $\Sigma_{2,0}/\Sigma_{1,0} = 1$ and $\sigma_{2,0}/\sigma_{1,0} = \frac{1}{2}$. These relations imply that $Q_{2,0} = \frac{1}{2}$ and $k_0 = \frac{1}{2}\,k_{J2,0}$, where $k_{J2,0} = 2\pi G\Sigma_{2,0}/\sigma_{2,0}^2$ is the Jeans wavenumber of component $i = 2$ (H_2) at scale $\ell = \ell_0$.

2.3.2 *H_2 in Regime C*

The response of H I is similar to the previous case, while H_2 behaves differently (see section 2.5 of Romeo et al. 2010). The self-gravity term gets dominant for large k and makes $\mathcal{M}_{H_2}^2(k)$ negative. So $\omega_-^2(k)$ is also negative in this limit (cf. Property I). For small k, $\mathcal{M}_{H_2}^2(k)$ is positive since it is dominated by the pressure term ($b > 1$) and/or the rotation term ($b \leq 1$). As neither $\mathcal{M}_{H_2}^2(k)$ nor $\mathcal{M}_{HI}^2(k)$ is driven by self-gravity at large scales, the right-hand side of equation (4) is negligible as $k \to 0$. So $\omega_-^2(k)$ is positive in this limit, like $\mathcal{M}_{HI}^2(k)$ and $\mathcal{M}_{H_2}^2(k)$. The disc is then unstable at small scales and stable at large scales, like H_2 itself (see the right-hand panel of Fig. 2).

2.3.3 *H_2 in Regime B*

The behaviour of H_2 is intermediate between the previous two cases (see section 2.3 of Romeo et al. 2010). A similar flow of arguments shows that the disc is in a phase of transition between stability in the manner of Toomre and instability at small scales, like H_2 itself. The middle panel of Fig. 2 illustrates the phase of small-scale instability, which occurs for $k_0 \leq k_{J2,0} = 2\pi G\Sigma_{H_2,0}/\sigma_{H_2,0}^2$ (see Hoffmann 2011 for a detailed analysis). Note how the two components contribute to the gravitational instability of the disc, and how their coupling widens the range of unstable scales.

2.4 Gas plus stars

This case involves three components: H I, H_2 and stars. In nearby spiral galaxies, H I and H_2 have distinct domains: H I dominates the outer regions of the gas disc, while H_2 dominates the inner regions (e.g. Leroy et al. 2008). We can then consider H I and H_2 separately. This makes sense here because we already know how the gravitational coupling between H I and H_2 modifies the main stability regimes of gas turbulence (see Section 2.3). What we now want to understand is the role that stars play in this stability scenario. Let us then distinguish two cases.

(i) *Stars plus H_2.* Since the stellar component populates Regime A (like H I) and H_2 populates Regimes A–C, this case is qualitatively similar to the set of cases analysed in Section 2.3. So there are three stability regimes: stability in the manner of Toomre, instability at small scales and a phase of stability transition. Note that such a variety of regimes is driven by H_2 turbulence. The stellar component can only modify the shape of the dispersion relation; it cannot change the type of stability regime. Note also that there is a mismatch between two important scales. One is the characteristic scale of stellar instabilities, $L_\star = \sigma_\star^2/\pi G\Sigma_\star$, which is typically $\sim$1 kpc (see, e.g., Binney & Tremaine 2008). The other is the largest scale at which H_2 turbulence has been observed, $L_{H_2} \sim 100$ pc (e.g. Bolatto et al. 2008). Since $L_\star$ is one order of magnitude larger than L_{H_2}, the stellar component cannot play a significant role in such stability regimes. Therefore, this is essentially a one-component case, driven and dominated by H_2. In Section 3, we will show that such stability regimes can indeed be frequent in nearby star-forming spirals.

(ii) *Stars plus H I.* As both components populate Regime A, this is a case of stability in the manner of Toomre: $\omega_-^2(k)$ has a global minimum, which determines whether the disc is stable for all wavenumbers or not (cf. Section 2.3.1). In contrast to case (i), H I turbulence reaches scales as large as 1–10 kpc (e.g. Kim et al. 2007; Dutta 2011). This makes it possible for the stellar component to 'interact' with H I turbulence and contribute significantly to two-fluid instabilities, as in the classical case of stars plus non-turbulent gas.

As discussed above, case (ii) represents the only stability regime in which stars play a non-negligible role. We then focus on this case, and analyse how gas turbulence affects the onset of gravitational instability in the disc, i.e. the local stability threshold and the corresponding characteristic wavelength. The effect of disc thickness is well known in this context (Romeo 1992, 1994; Elmegreen 2011; Romeo & Wiegert 2011). So we do not take that effect into account.

2.4.1 *The stability threshold*

As this is a Toomre-like case, the local stability criterion can be expressed in the usual form $Q_{\rm eff} \geq 1$, where $Q_{\rm eff}$ is the effective Q parameter. In the classical case of stars plus non-turbulent gas, $Q_{\rm eff}$ depends on three parameters: $Q_\star$, $Q_{\rm g}$ and $s = \sigma_{\rm g}/\sigma_\star$. For analysing $Q_{\rm eff}$ in detail, it is useful to factor out the dependence on $Q_\star$, $Q_{\rm eff} = Q_\star/\overline{Q}$, and study the stability threshold $\overline{Q}$ as a function of s and $q = Q_{\rm g}/Q_\star$ (Romeo & Wiegert 2011). When gas turbulence is taken into account via equation (3), $\overline{Q}$ depends on five parameters:

$$s_0 \equiv \frac{\sigma_{\rm g0}}{\sigma_\star}, \quad q_0 \equiv \frac{Q_{\rm g0}}{Q_\star}, \tag{9}$$

a, b and

$$\mathcal{L}_0 \equiv \ell_0\, k_{\rm T\star}, \tag{10}$$

where $k_{\rm T\star} = \kappa^2/2\pi G\Sigma_\star$ is the stellar Toomre wavenumber. A general five-parameter study of $\overline{Q}$ is not more useful than a targeted few-parameter analysis. This is because a, b and $\mathcal{L}_0$ are tightly constrained by observations, and because their observed values fall within a single stability regime (remember that this is a region of the parameter space where the disc has similar stability properties). For these reasons, we analyse $\overline{Q}$ as a function of s_0 and q_0, choosing observationally motivated values of a, b and $\mathcal{L}_0$: $a = b = \frac{1}{3}$, which is the typical scaling of H I turbulence (see Section 1), and $\mathcal{L}_0 = 1.0 \pm 0.5$, which are the median and 1σ scatter of $\mathcal{L}_0$ in the outer discs of THINGS spirals (where H I dominates; see Section 3). The range $0.5 \leq \mathcal{L}_0 \leq 1.5$ is also representative of clumpy galaxies at intermediate and high redshifts.[2]

Fig. 3 shows a contour map of the stability threshold $\overline{Q}$ for classical and turbulent discs. Consider the classical case first, and look at the contour levels $\overline{Q} = 1.1$ and 1.4. Their slope changes abruptly across the line $q_0 = 1$, showing that there are two distinct stability regimes. This fact has a simple explanation in terms of star–gas decoupling (Bertin & Romeo 1988; Romeo & Wiegert 2011). When $s_0 \lesssim 0.2$ and $q_0 \sim 1$, $\omega_-^2(k)$ has two minima: one at small k, where the response of the stellar component peaks, and the other at large k, where gas dominates. For $q_0 < 1$, the gaseous minimum is deeper than the stellar one, and therefore it controls the onset of disc instability. Vice versa, for $q_0 > 1$, it is the stellar minimum that determines the stability threshold. The line $q_0 = 1$ separates gas- from star-dominated regimes even when $s_0 \gtrsim 0.2$, but the transition is smooth in this case since $\omega_-^2(k)$ has a single minimum. In the turbulent case, each contour level is on average shifted down. As $\overline{Q}$ increases in the same direction, this means that turbulence lowers the stability threshold, i.e. it tends to stabilize the disc. In Section 3, we will evaluate the statistical significance of this effect.

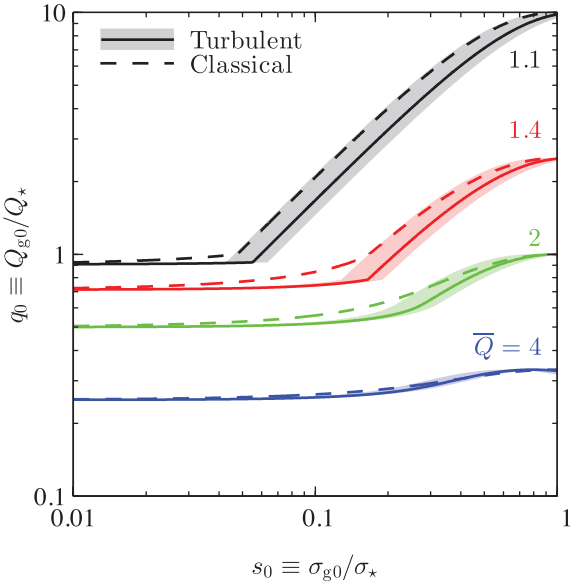

Figure 3. Contour lines of the stability threshold, $\overline{Q}(s_0, q_0) = \text{constant}$, for discs of stars and turbulent H I versus the classical case of stars plus non-turbulent gas. The solid lines and the shaded regions correspond to the median and the 1σ scatter of $\mathcal{L}_0$ in the outer discs of THINGS spirals.

2.4.2 *The characteristic wavelength*

The global minimum of $\omega_-^2(k)$ provides another useful stability diagnostic: the least stable wavelength $\lambda_{\rm min} = 2\pi/k_{\rm min}$ (see Jog 1996 for the classical case). When the disc is marginally stable, the value of $\lambda_{\rm min}$ is of particular interest. It is the wavelength at which instability first appears as $Q_\star$ drops below $\overline{Q}$. This wavelength can be written as $\overline{\lambda} = \overline{\Lambda}\,\lambda_{\rm T\star}$, where $\lambda_{\rm T\star} = 2\pi/k_{\rm T\star}$. The characteristic wavelength $\overline{\Lambda}$ depends on the same parameters as $\overline{Q}$. So we adopt the same approach as before, and analyse $\overline{\Lambda}$ as a function of s_0 and q_0 for observationally motivated values of a, b and $\mathcal{L}_0$.

Fig. 4 shows a contour map of the characteristic wavelength $\overline{\Lambda}$ for classical and turbulent discs. In the classical case, the contour levels $\overline{\Lambda} = 0.1$ and $\overline{\Lambda} = 0.2$ are truncated above $q_0 = 1$. This tells us that such short characteristic wavelengths occur only when stars and gas are decoupled and gas dominates. In fact, star-dominated instabilities appear at longer wavelengths: $\overline{\Lambda} \gtrsim 0.3$ (Bertin & Romeo 1988). Note also that the contour $\overline{\Lambda} = 0.5$ is a separatrix. Levels below 0.5 are on the left of this curve (and connected to the transition line), while levels above 0.5 are on the right. In the turbulent case, each contour level below 0.3 is on average shifted to the right, i.e. in the direction of increasing $\overline{\Lambda}$. This means that turbulence shortens the characteristic wavelength when stars and gas are decoupled and gas dominates. An opposite, although weaker, effect is detectable for $\overline{\Lambda} \geq 1$. Other regimes are also affected, but in a more complex way. This is especially true for $\overline{\Lambda} \sim 0.5$, since the separatrix of the parameter plane shifts to larger values. Last but not least, note how turbulence bends the transition line down, favouring star-dominated regimes. In Section 3, we will analyse these effects in detail.

[2] Puech (2010) analysed two such galaxy samples at $z \approx 0.6$ and $z \approx 2$. The median properties of the discs are summarized in his table 1 (see also his section 3.2). Using those data, we find that the stellar Toomre wavenumber is $k_{\rm T\star} \approx 0.3\,{\rm kpc}^{-1}$ at $z \approx 0.6$ and $k_{\rm T\star} \approx 0.2\,{\rm kpc}^{-1}$ at $z \approx 2$. The spatial resolution is $\ell_0 \approx 7$ kpc and $\ell_0 \approx 5$ kpc, respectively, in the two cases (Puech, private communication). This yields $\mathcal{L}_0 \approx 2$ at $z \approx 0.6$ and $\mathcal{L}_0 \approx 1$ at $z \approx 2$. Thus, even at intermediate and high redshifts, $\mathcal{L}_0$ is remarkably close to unity and lies within the 1σ scatter computed from THINGS.

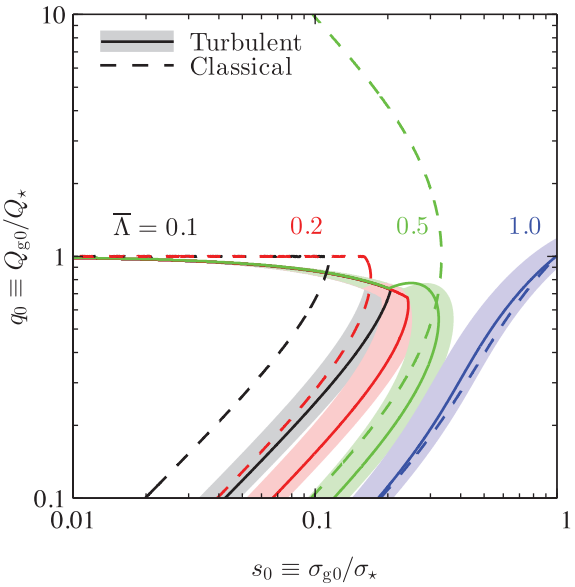

Figure 4. Contour lines of the characteristic wavelength, $\overline{\Lambda}(s_0, q_0) =$ constant, for discs of stars and turbulent H I versus the classical case of stars plus non-turbulent gas. The solid lines and the shaded regions correspond to the median and the 1σ scatter of $\mathcal{L}_0$ in the outer discs of THINGS spirals.

3 APPLICATION TO THINGS SPIRALS

We now consider a sample of 12 nearby star-forming spirals from THINGS: NGC 628, 3198, 3184, 4736, 3351, 6946, 3627, 5194, 3521, 2841, 5055 and 7331. For these galaxies, a detailed analysis by Leroy et al. (2008) provides high-quality measurements of kinematics, as well as stellar and gaseous surface densities, at a constant spatial resolution of 800 pc.

Leroy et al. (2008) also analysed the stability of those galaxies, treating the ISM as a single non-turbulent component, gravitationally coupled to stars, with surface density $\Sigma_g = \Sigma_{HI} + \Sigma_{H_2}$ and velocity dispersion $\sigma_g = 11\,\mathrm{km\,s^{-1}}$. Such a value of σ_g fits the H I data well, but is twice as large as the typical H_2 velocity dispersion observed in nearby spiral galaxies (Wilson et al. 2011). To represent both H I and H_2 well, we choose $\sigma_g = 8\,\mathrm{km\,s^{-1}}$. This value lies within the 1σ scatter of σ_{HI} ($11 \pm 3\,\mathrm{km\,s^{-1}}$; Leroy et al. 2008) and σ_{H_2} ($6.1 \pm 2.9\,\mathrm{km\,s^{-1}}$; Wilson et al. 2011), and therefore allows us to carry out an unbiased stability analysis of THINGS spirals.

The constant spatial resolution of 800 pc used by Leroy et al. (2008) makes their data particularly appropriate for analysing the effect of H I turbulence at galactic scales. H I dominates the gas surface density in the outer disc, typically for $R > 0.43\,R_{25}$, where R_{25} is the optical radius (Leroy et al. 2008). We then treat gas as turbulent for $R > 0.43\,R_{25}$, and assume Larson-type scaling relations (see equation 3) with $\ell_0 = 800\,\mathrm{pc}$, $\Sigma_{g0} = \Sigma_{g0}(R)$ as tabulated by Leroy et al. (2008), and $\sigma_{g0} = 8\,\mathrm{km\,s^{-1}}$ (see above). Concerning a and b, we analyse the case $a = b = \frac{1}{3}$ in detail, since it represents H I observations fairly well (see Section 1). We have also studied the case $a = b = \frac{1}{2}$, as representative of high-resolution simulations of supersonic turbulence (see Section 1), but here we will only mention it when discussing the results of our stability analysis. Hereafter, we will refer to the model described above as *Model 1*.

3.1 The condition for star–gas decoupling

In Section 2.4, we have seen that there is a region in the parameter plane where $\omega_-^2(k)$ has two minima. This is the 'two-phase region' introduced by Bertin & Romeo (1988) and further investigated by Romeo & Wiegert (2011).

Fig. 5 shows the two-phase region for classical and turbulent discs. Within this region, stars and gas are dynamically decoupled and the disc is susceptible to instabilities at two different wavelengths, where the responses of the two components peak. In the stellar phase, the disc is more susceptible to long-wavelength instabilities, whereas in the gaseous phase it is dominated by short-wavelength instabilities. Along the transition line between the phases, neither component dominates and instabilities occur both at short and at long wavelengths. Outside the two-phase region, the two components are strongly coupled and instabilities occur at intermediate wavelengths.

We populate the parameter plane with measurements taken from the sample of spiral galaxies, and colour-code them by radius. We draw the turbulent two-phase region corresponding to the median and 1σ scatter of $\mathcal{L}_0$ for $R > 0.43\,R_{25}$. Note the following points.

(i) The two-phase region of a classical disc is symmetric about $q = 1$. This symmetry is broken for a turbulent disc because gas (dominant for $q < 1$) follows turbulent scaling, but stars (dominant for $q > 1$) do not.

(ii) The turbulent two-phase region is larger than the classical one. This follows from the fact that turbulence pushes the minima of $\omega_-^2(k)$ further apart, and the maximum between them further up, so as to favour star–gas decoupling.

(iii) The transition line appears unaffected by the scatter of $\mathcal{L}_0$. This is because the shape of the two-phase region depends on s and q, and q is not affected by turbulence ($q = q_0$) if $a = b$.

(iv) Turbulence increases the size of the stellar phase more than that of the gaseous phase. Recall that the boundary of the two-phase region is marked by the disappearance of the non-dominant peak, i.e. the gas peak in the stellar phase and vice versa. Since turbulence affects the gaseous peak more than the stellar peak, the size of the stellar phase is affected more than that of the gaseous phase. For $R > 0.43\,R_{25}$, this causes a significant number of measurements to populate the stellar phase.

(v) For $R \leq 0.43\,R_{25}$, we find that $f_2 = 61$ per cent of all points populate the two-phase region, two-thirds of them in the gaseous phase. In such cases, the onset of gravitational instability is controlled by H_2. Turbulence is expected to play an important role in this process at scales smaller than about 100 pc (see Section 2.4). For $R > 0.43\,R_{25}$, only 4 per cent of all points populate this region for a classical disc. This fraction increases to 22 per cent for a turbulent disc with $a = b = \frac{1}{3}$, and to 52 per cent for $a = b = \frac{1}{2}$.

3.2 The effective Q parameter

Fig. 6 shows radial profiles of the effective Q parameter, $Q_{\mathrm{eff}} = Q_{\mathrm{eff}}(R)$, for our sample of galaxies. In the left-hand panel, we neglect gas turbulence. On the right, we consider turbulent H I ($a = b = \frac{1}{3}$) for $R > 0.43\,R_{25}$. Values of Q_{eff} smaller than unity mean gravitational instability. We indicate the median and 1σ scatter of Q_{eff} for radii smaller and larger than $R = 0.43\,R_{25}$. We also colour-code the component that contributes more to disc instability according to the classical condition: gas for $Q_{g_0} < Q_\star$ and stars for $Q_\star < Q_{g_0}$ (Romeo & Wiegert 2011).

For $R \leq 0.43\,R_{25}$, Q_{eff} spans a wide range of values, with 13 per cent of points in the unstable regime. Here 56 per cent of points

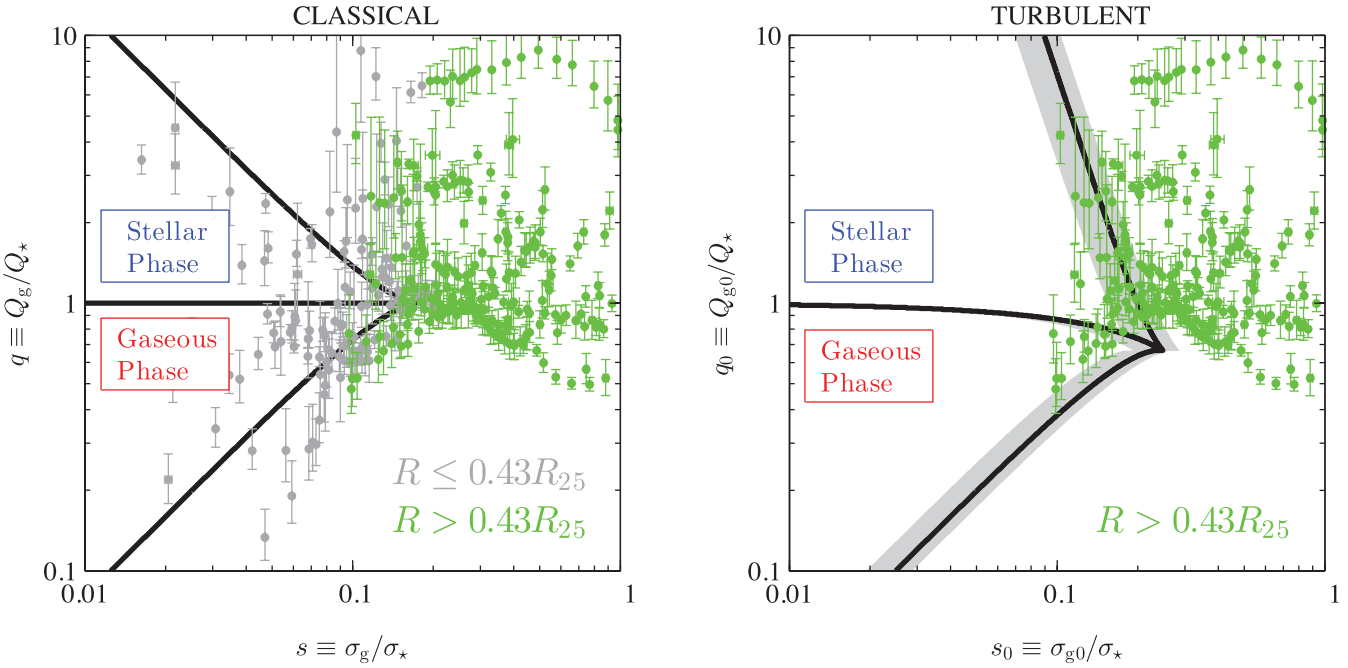

Figure 5. The parameter plane populated by THINGS spirals (Model 1), and the 'two-phase region' where stars and gas contribute separately to the gravitational instability of the disc: neglecting gas turbulence (left), and taking into account H I turbulence for $R > 0.43\,R_{25}$ (right). In the turbulent case, the solid lines and the shaded regions correspond to the median and the 1σ scatter of $\mathcal{L}_0$ in that radial range. Data from THINGS are coloured according to the dominant component: H_2 for $R \leq 0.43\,R_{25}$, and H I for $R > 0.43\,R_{25}$.

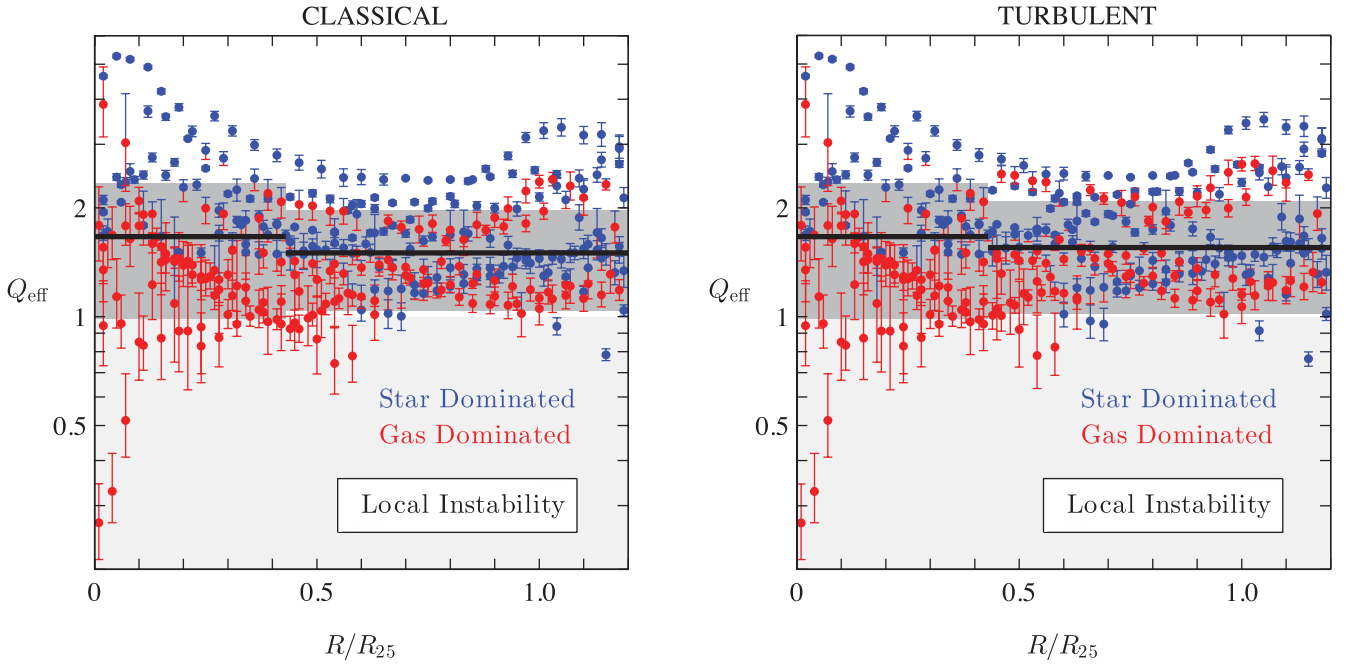

Figure 6. Radial profile of the effective Q parameter, $Q_{\rm eff}(R)$, for THINGS spirals (Model 1): neglecting gas turbulence (left), and taking into account H I turbulence for $R > 0.43\,R_{25}$ (right). The disc is locally unstable for $Q_{\rm eff} < 1$ (light grey shading). For each measurement, we indicate whether the stability level is dominated by the stellar ($Q_\star < Q_{g_0}$) or the gaseous ($Q_{g_0} < Q_\star$) component. The thick black lines and dark grey shading indicate the median and 1σ scatter of $Q_{\rm eff}$ in the two radial ranges.

are gas dominated and tend to be less stable than the star-dominated points (the median value of $Q_{\rm eff}$ is $Q_{{\rm eff},g} \approx 1.3$ and $Q_{{\rm eff},\star} \approx 2.3$ in the two cases). For $R > 0.43\,R_{25}$, the range spanned by $Q_{\rm eff}$ is tighter and only 4 per cent of measurements are in the unstable regime. Here the majority (61 per cent) of points are star dominated, and there is no clear difference in $Q_{\rm eff}$ between star- and gas-dominated points ($Q_{{\rm eff},g} \approx 1.3$ and $Q_{{\rm eff},\star} \approx 1.7$).

Introducing turbulent scaling for $R > 0.43, R_{25}$ only has a small effect on the measurements. For $a = b = \frac{1}{3}$, the median of $Q_{\rm eff}$ increases by 3 per cent and the 1σ scatter by 15 per cent.

For $a = b = \frac{1}{2}$, the median increases by 6 per cent and the 1σ scatter by 26 per cent. This suggests that turbulence tends to stabilize the disc (the median increases), although the magnitude of this effect is small and depends on the non-turbulent value of $Q_{\rm eff}$ (the scatter increases).

The stabilizing effect of turbulence seems at odds with results from Romeo et al. (2010), who found that the stability of gaseous discs is unaffected by turbulence if $a = b$. The difference lies, of course, in the gravitational coupling of stars and gas. Consider the approximation for the effective Q parameter introduced by Romeo & Wiegert (2011):

$$\frac{1}{Q_{\rm eff}} = \begin{cases} \dfrac{W}{Q_\star} + \dfrac{1}{Q_{\rm g}} \text{ if } Q_\star \geq Q_{\rm g}\,, \\ \dfrac{1}{Q_\star} + \dfrac{W}{Q_{\rm g}} \text{ if } Q_{\rm g} \geq Q_\star\,, \end{cases} \tag{11}$$

$$W = \frac{2\sigma_\star\sigma_{\rm g}}{\sigma_\star^2 + \sigma_{\rm g}^2}\,. \tag{12}$$

We see that, even if $Q_{\rm g} = Q_{\rm g_0}$, the scaling $\sigma_{\rm g} = \sigma_{\rm g_0}(\ell/\ell_0)^b$ affects the weight factor $W(\sigma_\star, \sigma_{\rm g})$. The strength of this effect is determined by the power-law slope b. Therefore, the effective Q parameter of turbulent discs always differs from the classical case.

3.3 The least stable wavelength

Fig. 7 shows radial profiles of the least stable wavelength, $\lambda_{\rm min} = \lambda_{\rm min}(R)$, for our sample. On the left, we neglect gas turbulence, whereas on the right we consider turbulent H I for $R > 0.43\,R_{25}$. Colour-coding indicates the component that dominates gravitational instability. As before, the median and 1σ scatter are indicated separately for small and large radii.

For $R \leq 0.43\,R_{25}$, there is a clear gap between gas- and star-dominated points (the median value of $\lambda_{\rm min}$ is $\lambda_{\rm min,g} \approx 0.7$ kpc and $\lambda_{\rm min,\star} \approx 8.2$ kpc in the two cases). So the gas-dominated points are characterized by much smaller values of $\lambda_{\rm min}$. The discrepancy is less significant for $R > 0.43\,R_{25}$, apart from a few measurements close to $R = 0.43\,R_{25}$ ($\lambda_{\rm min,g} \approx 3.9$ kpc and $\lambda_{\rm min,\star} \approx 6.3$ kpc).

Introducing a turbulent gas component for $R > 0.43\,R_{25}$ causes a significant increase in $\lambda_{\rm min}$. For $a = b = \frac{1}{3}$, the median of $\lambda_{\rm min}$ increases by 28 per cent and the 1σ scatter by 34 per cent. For $a = b = \frac{1}{2}$, the median increases by 41 per cent and the increase in 1σ scatter is again 34 per cent. This suggests a tendency of turbulence to boost the least stable wavelength. As for $Q_{\rm eff}$, the magnitude of this effect depends on the non-turbulent value of $\lambda_{\rm min}$. There is a small number of gas-dominated measurements for which the least stable wavelength decreases, but these have large uncertainties.

Why does turbulence affect $\lambda_{\rm eff}$ more than $Q_{\rm eff}$? The answer is twofold. First, for a purely gaseous disc, $\lambda_{\rm min}$ increases markedly with $Q_{\rm eff}$ (Romeo et al. 2010), so that any change in $Q_{\rm eff}$ will be amplified in $\lambda_{\rm min}$. Secondly, as stars are taken into account, gas-dominated points can enter the star-dominated regime, where $\lambda_{\rm min}$ is much larger (see Section 2.4). Both effects depend on the power-law slopes a and b. They sum up and drive $\lambda_{\rm min}$ to significantly larger values.

3.4 Robustness of the results

Modelling the gas disc as a single component with an intermediate value of $\sigma_{\rm g}$ is not the best that can be done. Here we will no longer follow this traditional approach. We will model the gas disc as made of two components, each with the more representative value of $\sigma_{\rm g}$. A simple way to do it is to treat the inner part of the disc as H_2 dominated and the outer part as H I dominated. We then set $\sigma_{\rm g} = 6\,{\rm km\,s^{-1}}$ for $R \leq 0.43\,R_{25}$ and $\sigma_{\rm g} = 11\,{\rm km\,s^{-1}}$ for $R > 0.43\,R_{25}$ (cf. the introductory part of Section 3).

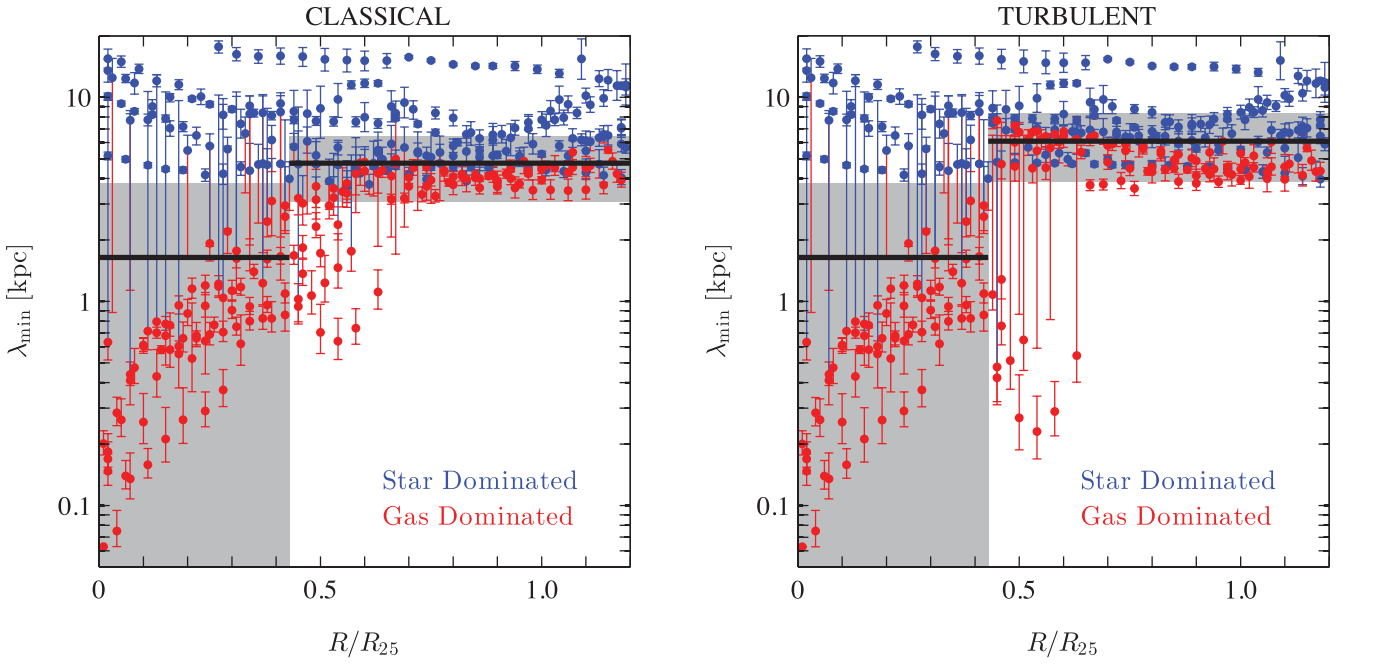

Figure 7. Radial profile of the least stable wavelength, $\lambda_{\rm min}(R)$, for THINGS spirals (Model 1): neglecting gas turbulence (left) and taking into account H I turbulence for $R > 0.43\,R_{25}$ (right). For each measurement, colour-coding indicates whether gas ($Q_{\rm g_0} < Q_\star$) or stars ($Q_\star < Q_{\rm g_0}$) dominate the stability level. The thick black lines and dark grey shading indicate the median and 1σ scatter of $\lambda_{\rm min}$ in the two radial ranges.

Table 1. Stability characteristics of THINGS spirals for Models 1 and 2.

Model	Radial range	a	b	f_2 [a] (per cent)	$f_{2,g}$ [b] (per cent)	f_u [c] (per cent)	f_g [d] (per cent)	Q_{eff} [e]	λ_{min} [f] (kpc)
1	$R \leq 0.43\,R_{25}$	0	0	61	68	13	56	1.67 ± 0.68	1.64 ± 2.17
	$R > 0.43\,R_{25}$	0	0	4	100	4	39	1.50 ± 0.46	4.76 ± 1.67
		1/3	1/3	22	41	3	39	1.55 ± 0.53	6.10 ± 2.24
		1/2	1/2	52	9	3	39	1.59 ± 0.58	6.70 ± 2.23
2	$R \leq 0.43\,R_{25}$	0	0	73	76	25	77	1.50 ± 0.91	0.67 ± 0.62
	$R > 0.43\,R_{25}$	0	0	4	100	0.5	39	1.99 ± 0.57	9.32 ± 3.40
		1/3	1/3	19	48	0.5	39	2.09 ± 0.66	11.10 ± 2.78
		1/2	1/2	52	5	0.5	39	2.14 ± 0.72	12.00 ± 2.43

[a]Fraction of data that fall within the two-phase region.
[b]Fraction of the data points in [a] that populate the gaseous phase.
[c]Fraction of data such that $Q_{eff} < 1$.
[d]Fraction of data such that $Q_{g0} < Q_\star$.
[e]Median and 1σ scatter of Q_{eff}.
[f]Median and 1σ scatter of λ_{min}.

Besides σ_g, there is another quantity that deserves particular attention: the stellar radial velocity dispersion, which we now denote with $\sigma_{R\star}$. Leroy et al. (2008) inferred $\sigma_{R\star}$ from the vertical velocity dispersion, $\sigma_{z\star}$, assuming that $(\sigma_z/\sigma_R)_\star = 0.6$. In turn, $\sigma_{z\star}$ was inferred from the stellar exponential scale height, $H_\star$, using the relation $H_\star = \sigma_{z\star}^2/2\pi G\Sigma_\star$. Gerssen & Shapiro Griffin (2012) showed that $(\sigma_z/\sigma_R)_\star$ decreases markedly from early- to late-type spirals. The average Hubble stage of THINGS spirals is $\langle T\rangle = 4$, which corresponds to galaxy type Sbc (the mean and the median of T are equal). The best-fitting model of Gerssen & Shapiro Griffin (2012) then yields $(\sigma_z/\sigma_R)_\star = 0.5$ (see their fig. 4). Concerning $H_\star$, the relation used by Leroy et al. (2008) is not correct. It is the total surface density in the disc that determines the stellar exponential scale height: $H_\star = \sigma_{z\star}^2/2\pi G\Sigma_{tot}$, where $\Sigma_{tot} = \Sigma_\star + \Sigma_g$ (Bahcall & Casertano 1984; Romeo 1992). In view of these facts, we set $(\sigma_z/\sigma_R)_\star = 0.5$ and use the correct relation for $H_\star$.

Finally, we implement gas turbulence as in model 1, i.e. only for $R > 0.43\,R_{25}$, where the disc is H I dominated. This is simply because the constant spatial resolution of 800 pc used by Leroy et al. (2008) is too coarse to probe the range of scales affected by H_2 turbulence [see Section 2.4, case (i)]. Hereafter, we will refer to the model described above as *Model 2*.

Table 1 summarizes the dynamical differences between Model 2 and Model 1. On the whole, the stability diagnostics are moderately affected by the model. The most sensitive diagnostic is λ_{min}, which differs by a factor of 2–3. Q_{eff} is more robust, with a difference well below a factor of 2. In Model 2, both λ_{min} and Q_{eff} are smaller for $R \leq 0.43\,R_{25}$ and larger for $R > 0.43\,R_{25}$.

Despite these differences, the effect of turbulence is comparable in the two models. For $R \leq 0.43\,R_{25}$, f_2 and $f_{2,g}$ are slightly larger in Model 2. So H_2 is more decoupled from stars and slightly more dominant. For $R > 0.43\,R_{25}$, f_2 is almost identical in the two models, irrespective of the value of $a = b$. Turbulence increases the median value of Q_{eff} by less than 10 per cent in both models. In contrast, the median value of λ_{min} increases by 20–30 per cent in Model 2, i.e. less than in Model 1. Summarizing, the effect of H I turbulence in Model 2 is only slightly weaker than in Model 1. This points to the robustness of our results.

4 DISCUSSION

Our results cannot be directly compared with those of Shadmehri & Khajenabi (2012), hereafter SK12. This is partly because of the wider scope of our paper, which embraces a brand new application to THINGS spirals, and because most of the analysis carried out by SK12 cannot be easily interpreted.

SK12 analysed five stability regimes of gas turbulence: $a > 1$ and $b < \frac{1}{2}(1+a)$; $a = 1$ and $b \neq 1$; and Regimes A–C. The first regime corresponds to a fractal dimension $D = a + 2$ higher than 3, and is therefore beyond the natural range of a (see fig. 1 and section 3 of Romeo et al. 2010). In the second regime, the volume density is scale independent ($D = 3$), so the medium is incompressible and hence subsonic. Cold interstellar gas is instead dominated by compressible structures and supersonic motions. Therefore, even this regime is of marginal interest (see again fig. 1 and section 3 of Romeo et al. 2010). Regimes B and C are populated by H_2 turbulence, which manifests itself at scales less than $L_{H_2} \sim 100$ pc. In turn, L_{H_2} is one order of magnitude smaller than the characteristic scale of stellar instabilities. Therefore, stars play a negligible role in these stability regimes [see Section 2.4, case (i)]. SK12 reached the opposite conclusion. But this is because they assumed Larson-type scaling relations even at kpc scales, disregarding the type of turbulence associated with such regimes. Regime A is populated by both H_2 and H I turbulence. While the H_2 case raises the same issue as Regimes B and C, the H I case is conceptually simpler. H I turbulence manifests itself at all scales of galactic interest, so stars can play a significant role in this stability regime [see Section 2.4, case (ii)]. SK12 reached a similar conclusion. However, even in this case, their approach is different from ours. They chose a, b and $\mathcal{L}_0$ so as to sample Regime A, and studied the dispersion relation numerically. We have instead examined the whole regime analytically (see Section 2.3.1). We have then chosen observationally motivated values of a, b and $\mathcal{L}_0$, and analysed the onset of gravitational instability in the disc (see in particular Sections 2.4.1 and 2.4.2).

In conclusion, there is a fundamental difference between our analysis and that of SK12. Our analysis takes into account the astrophysical relevance of the various stability regimes, as well as the tight constraints imposed by observations of ISM turbulence in the Milky Way and nearby galaxies. These are important aspects of the problem, which are missing from their analysis.

5 CONCLUSIONS

Our analysis of THINGS spirals shows that H I turbulence has a triple effect on the outer regions of galactic discs: (i) it weakens the coupling between gas and stars in the development of disc

instabilities, (ii) it makes the disc more prone to star-dominated than gas-dominated instabilities and (iii) it typically increases the least stable wavelength by 20–40 per cent (the steeper the H I scaling relations, the larger the effect). This is in contrast to the typical 3–8 per cent increase predicted for the effective Q parameter. The effect of H I turbulence is in a sense complementary to the effect of disc thickness. In fact, disc thickness increases the effective Q parameter by 20–50 per cent (Romeo & Wiegert 2011) but hardly changes the least stable wavelength (Romeo 1992, 1994) or the condition for star–gas decoupling (Romeo & Wiegert 2011).

Our analysis of THINGS spirals also suggests that H_2 turbulence has a significant effect on the inner regions of galactic discs. For $R \lesssim 0.4\,R_{25}$, i.e. where H_2 dominates over H I, 60–70 per cent of the data fulfil the condition for star–gas decoupling and 70–80 per cent of these points represent gas-dominated stability regimes. In such cases, the onset of gravitational instability is controlled by H_2. Turbulence is expected to play an important role in this process at scales smaller than about 100 pc (see Section 2.4). If $a = 0$ and $b = \frac{1}{2}$, then H_2 turbulence drives the disc to a regime of transition between instability at small scales and stability in the manner of Toomre, as was first pointed out by Romeo et al. (2010) in the case of one-component turbulent discs. Since this is a regime of transition, even small deviations from the standard H_2 scaling laws ($a = 0$ and $b = \frac{1}{2}$) can have a strong impact on the gravitational instability of the disc. This is true even when the mass densities of H I and H_2 are comparable, since small-scale instabilities are more actively controlled by H_2 (see Section 2.3).

ACKNOWLEDGMENTS

We are very grateful to Oscar Agertz, Christoph Federrath, Mathieu Puech and Joachim Wiegert for useful discussions. We are also grateful to an anonymous referee for constructive comments and suggestions, and for encouraging future work on the topic. ABR thanks the warm hospitality of both the Department of Physics at the University of Gothenburg and the Department of Fundamental Physics at Chalmers.

REFERENCES

Agertz O., Lake G., Teyssier R., Moore B., Mayer L., Romeo A. B., 2009, MNRAS, 392, 294
Azimlu M., Fich M., 2011, AJ, 141, 123
Bahcall J. N., Casertano S., 1984, ApJ, 284, L35
Ballesteros-Paredes J., Hartmann L. W., Vázquez-Semadeni E., Heitsch F., Zamora-Avilés M. A., 2011, MNRAS, 411, 65
Beaumont C. N., Goodman A. A., Alves J. F., Lombardi M., Román-Zúñiga C. G., Kauffmann J., Lada C. J., 2012, MNRAS, 423, 2579
Begum A., Chengalur J. N., Bhardwaj S., 2006, MNRAS, 372, L33
Bertin G., Romeo A. B., 1988, A&A, 195, 105
Binney J., Tremaine S., 2008, Galactic Dynamics. Princeton Univ. Press, Princeton
Block D. L., Puerari I., Elmegreen B. G., Bournaud F., 2010, ApJ, 718, L1
Bolatto A. D., Leroy A. K., Rosolowsky E., Walter F., Blitz L., 2008, ApJ, 686, 948
Bournaud F., Elmegreen B. G., Teyssier R., Block D. L., Puerari I., 2010, MNRAS, 409, 1088
Cacciato M., Dekel A., Genel S., 2012, MNRAS, 421, 818
Collins D. C., Kritsuk A. G., Padoan P., Li H., Xu H., Ustyugov S. D., Norman M. L., 2012, ApJ, 750, 13
Combes F. et al., 2012, A&A, 539, A67
Dutta P., 2011, PhD thesis, Indian Institute of Technology, Kharagpur, India
Dutta P., Begum A., Bharadwaj S., Chengalur J. N., 2008, MNRAS, 384, L34
Dutta P., Begum A., Bharadwaj S., Chengalur J. N., 2009a, MNRAS, 397, L60
Dutta P., Begum A., Bharadwaj S., Chengalur J. N., 2009b, MNRAS, 398, 887
Dutta P., Begum A., Bharadwaj S., Chengalur J. N., 2010, MNRAS, 405, L102
Elmegreen B. G., 1995, MNRAS, 275, 944
Elmegreen B. G., 1996, in Block D. L., Greenberg J. M., eds, New Extragalactic Perspectives in the New South Africa. Kluwer, Dordrecht, p. 467
Elmegreen B. G., 2011, ApJ, 737, 10
Elmegreen B. G., Scalo J., 2004, ARA&A, 42, 211
Elmegreen B. G., Kim S., Staveley-Smith L., 2001, ApJ, 548, 749
Federrath C., Klessen R. S., Schmidt W., 2009, ApJ, 692, 364
Federrath C., Roman-Duval J., Klessen R. S., Schmidt W., Mac Low M.-M., 2010, A&A, 512, A81
Field G. B., Blackman E. G., Keto E. R., 2011, MNRAS, 416, 710
Fleck R. C., Jr, 1996, ApJ, 458, 739
Forbes J., Krumholz M., Burkert A., 2012, ApJ, 754, 48
Gerssen J., Shapiro Griffin K., 2012, MNRAS, 423, 2726
Heyer M., Krawczyk C., Duval J., Jackson J. M., 2009, ApJ, 699, 1092
Hoffmann V., 2011, MSc thesis, Chalmers University of Technology, Gothenburg, Sweden
Hughes A. et al., 2010, MNRAS, 406, 2065
Jog C. J., 1996, MNRAS, 278, 209
Jog C. J., Solomon P. M., 1984a, ApJ, 276, 114
Jog C. J., Solomon P. M., 1984b, ApJ, 276, 127
Kauffmann J., Pillai T., Shetty R., Myers P. C., Goodman A. A., 2010, ApJ, 716, 433
Kim S. et al., 2007, ApJS, 171, 419
Kowal G., Lazarian A., 2007, ApJ, 666, L69
Kowal G., Lazarian A., Beresnyak A., 2007, ApJ, 658, 423
Kritsuk A. G., Norman M. L., 2011, preprint (arXiv:1111.2827)
Kritsuk A. G., Norman M. L., Padoan P., Wagner R., 2007, ApJ, 665, 416
Larson R. B., 1981, MNRAS, 194, 809
Lazarian A., Pogosyan D., 2000, ApJ, 537, 720
Leroy A. K., Walter F., Brinks E., Bigiel F., de Blok W. J. G., Madore B., Thornley M. D., 2008, AJ, 136, 2782
Lin C. C., Shu F. H., 1966, Proc. Natl. Acad. Sci. USA, 55, 229
Lombardi M., Alves J., Lada C. J., 2010, A&A, 519, L7
McKee C. F., Ostriker E. C., 2007, ARA&A, 45, 565
Price D. J., Federrath C., 2010, MNRAS, 406, 1659
Puech M., 2010, MNRAS, 406, 535
Rafikov R. R., 2001, MNRAS, 323, 445
Roman-Duval J., Federrath C., Brunt C., Heyer M., Jackson J., Klessen R. S., 2011, ApJ, 740, 120
Romeo A. B., 1992, MNRAS, 256, 307
Romeo A. B., 1994, A&A, 286, 799
Romeo A. B., Wiegert J., 2011, MNRAS, 416, 1191
Romeo A. B., Burkert A., Agertz O., 2010, MNRAS, 407, 1223
Roy N., Peedikakkandy L., Chengalur J. N., 2008, MNRAS, 387, L18
Sánchez N., Añez N., Alfaro E. J., Odekon M. C., 2010, ApJ, 720, 541 (erratum: ApJ, 723, 969)
Schmidt W., Federrath C., Klessen R., 2008, Phys. Rev. Lett., 101, 194505
Shadmehri M., Khajenabi F., 2012, MNRAS, 421, 841 (SK12)
Shen Y., Lou Y.-Q., 2003, MNRAS, 345, 1340
Solomon P. M., Rivolo A. R., Barrett J., Yahil A., 1987, ApJ, 319, 730
Swinbank A. M. et al., 2011, ApJ, 742, 11
Toomre A., 1964, ApJ, 139, 1217
Vandervoort P. O., 1970, ApJ, 161, 87
Wilson C. D. et al., 2011, MNRAS, 410, 1409
Zhang H.-X., Hunter D. A., Elmegreen B. G., 2012, ApJ, 754, 29

This paper has been typeset from a TEX/LATEX file prepared by the author.